**SUPPORTING INFORMATION**

# Induced Dipole-Dipole Interactions Influence the Unfolding Pathways of Wild-Type and Mutant Amyloid β-Peptides

Justin A. Lemkul, Jing Huang, and Alexander D. MacKerell, Jr.

*Department of Pharmaceutical Sciences*
*School of Pharmacy, University of Maryland, Baltimore*

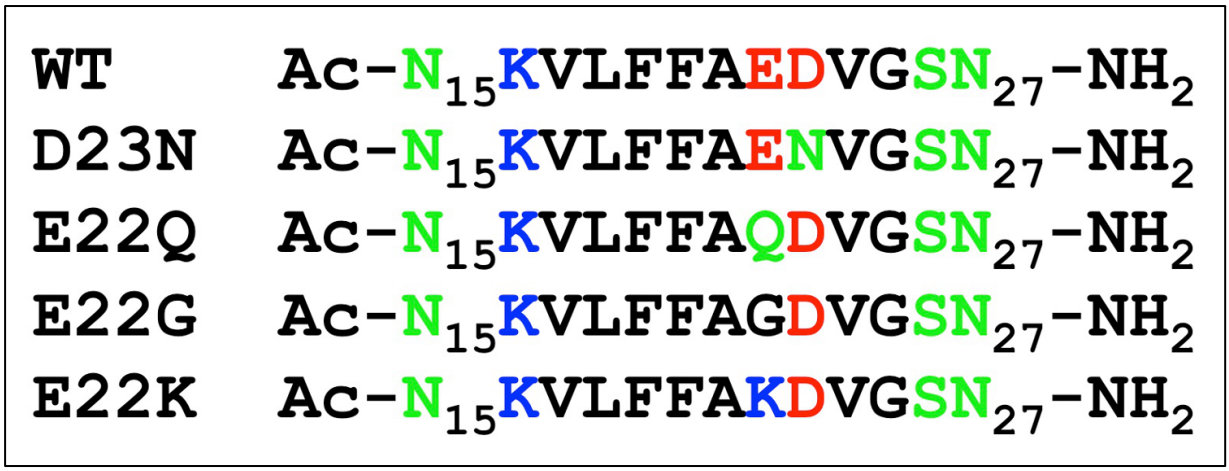


**Figure S1.** Sequences of the WT and mutant $A\beta_{15-27}$ peptides studied in the present work. Amino acids are colored according to the chemical nature of their side chains, blue for positively charged, red for negatively charged, green for neutral polar, and black for hydrophobic and glycine (no side chain).

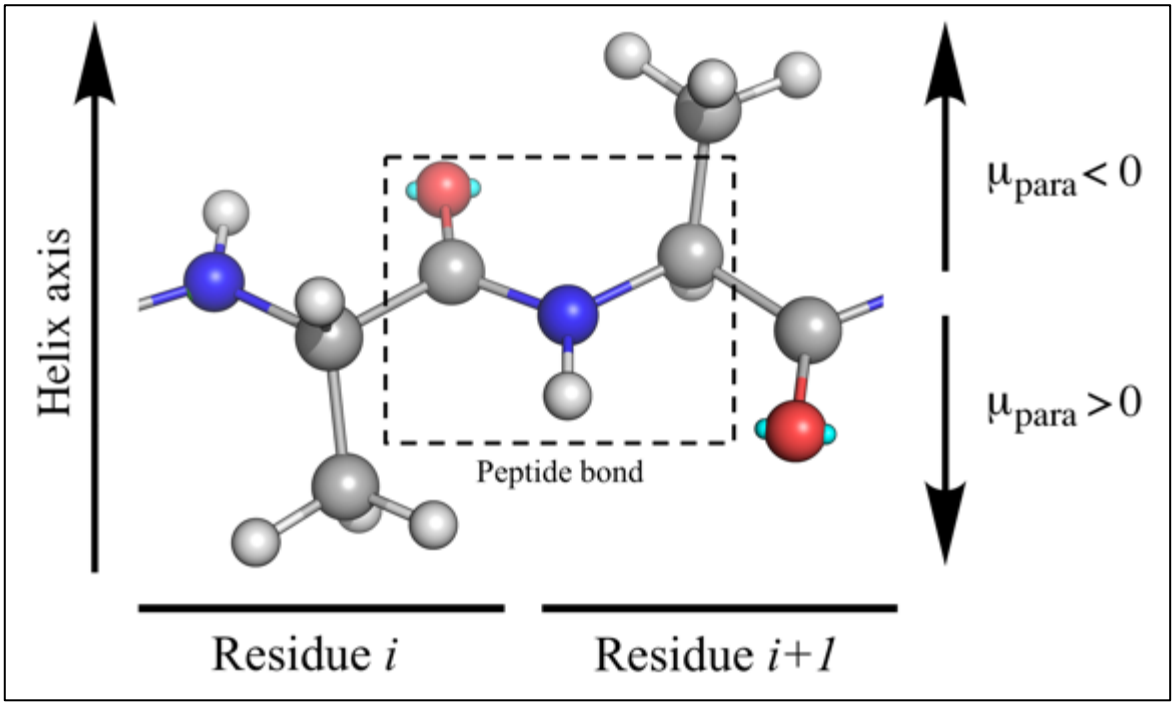


**Figure S2.** Definition of the peptide bond used for the dipole moment analysis, helix axis, and $\mu_{para}$ convention.

**Table S1.** Average α-helix content (given as a percentage of all residues in α-helical conformations) for all 300-ns trajectories. For this analysis, the definition of an α-helical residue was that of DSSP, which assigns secondary structure based on hydrogen bonding patterns, thus allowing for per-residue analysis to better correspond to experimental results.

| | Drude | | CHARMM36 | |
|---|---|---|---|---|
| | Water | Ethanol | Water | Ethanol |
| WT | 19.7 | 10.2 | 31.5 | 54.9 |
| D23N | 18.6 | 70.1 | 40.5 | 75.5 |
| E22Q | 15.6 | 62.4 | 6.2 | 53.9 |
| E22G | 13.6 | 43.1 | 7.1 | 57.3 |
| E22K | 23.3 | 49.7 | 53.4 | 72.8 |

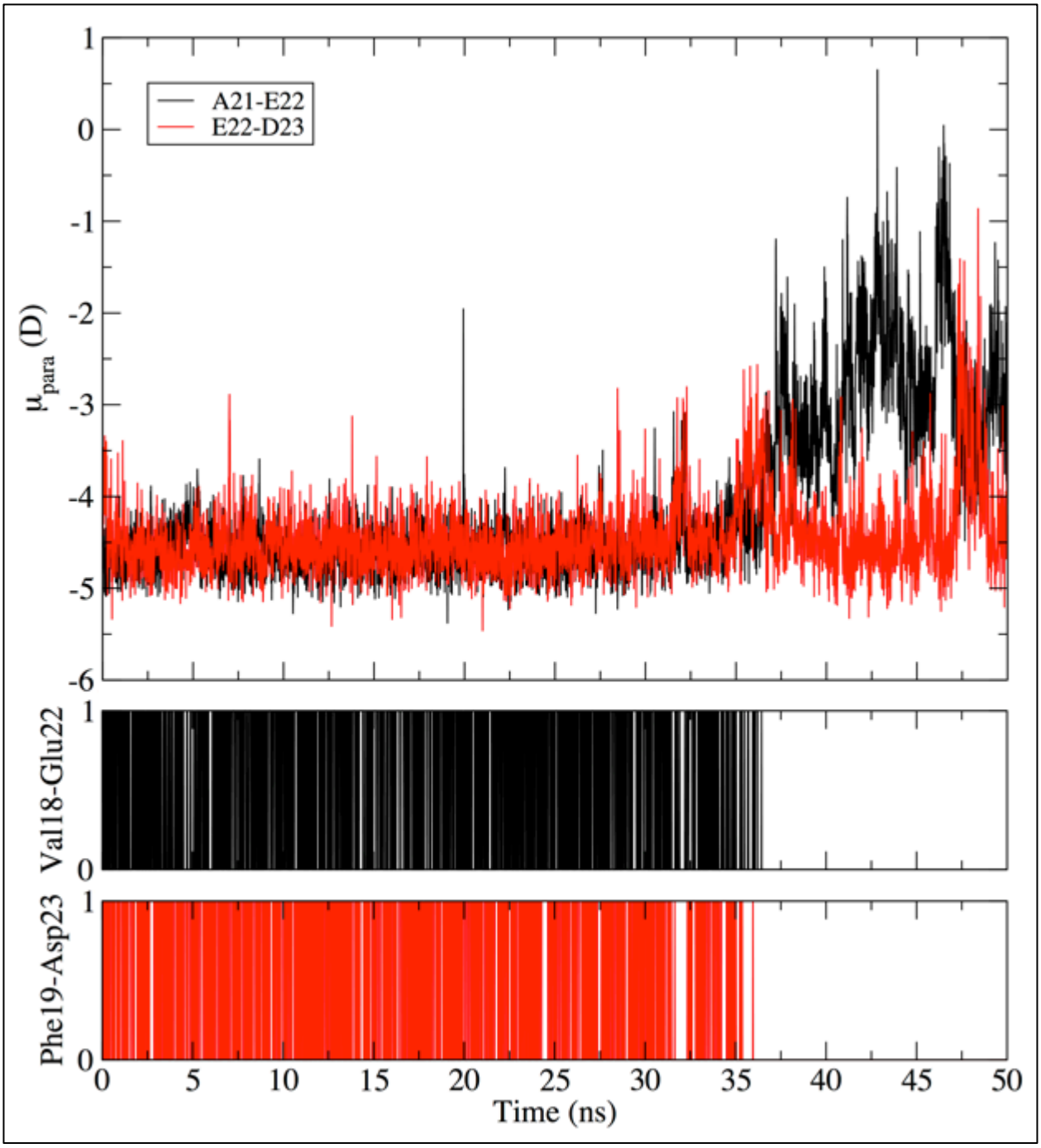


**Figure S3.** Response of peptide-bond dipole moments and hydrogen bond existence from simulations of WT $A\beta_{15-27}$ in water. The component of the peptide-bond dipole moment parallel to the helix axis ($\mu_{para}$) for each of the indicated peptide bonds is shown, focusing on the first 50 ns to illustrate the relationship between hydrogen bond dynamics and the dipole moments. Black or red spikes indicate the presence of a hydrogen bond (i.e. hydrogen bond existence = 1), according to the criteria of donor - acceptor distance ≤ 3.5 Å and donor - hydrogen - acceptor angle ≥ 150°.

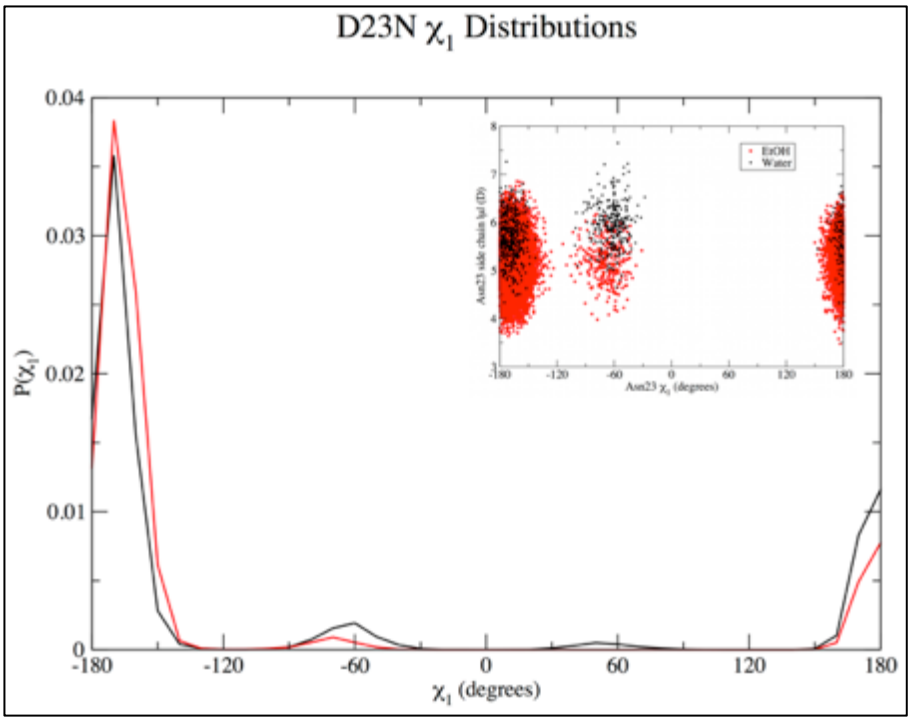


**Figure S4.** Asn23 $\chi_1$ distributions for D23N $A\beta_{15-27}$ in water (black) and ethanol (red). The inset shows the Asn23 side chain dipole moment as a function of $\chi_1$, considering only frames in which Asn23 was in an $\alpha$-helix.

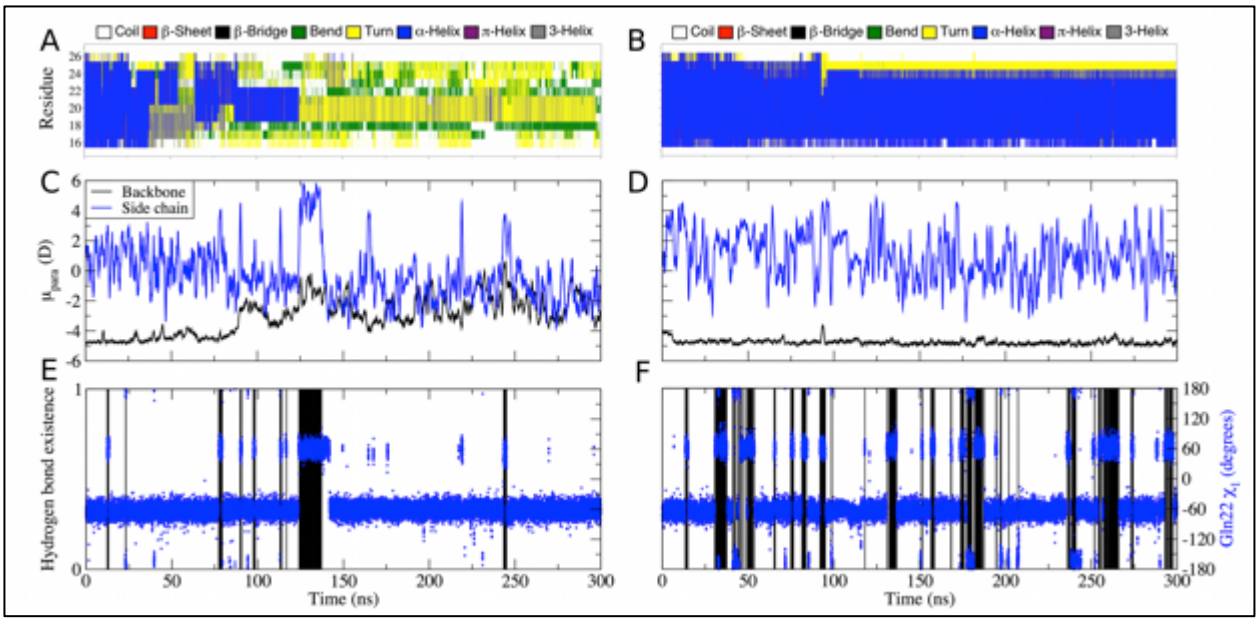


**Figure S5.** Secondary structure evolution for E22Q $A\beta_{15-27}$ according to the DSSP algorithm in (A) water and (B) ethanol. $\mu_{para}$ for the Gln22 side chain (blue) and Gln22-Asp23 backbone peptide bond (black) in (C) water and (D) ethanol, shown as 1-ns running averages for clarity. The legend in panel (C) also applies to panel (D). The Gln22 side chain $\chi_1$ time series (blue dots) in (E) water and (F) ethanol are shown as a function of the Gln22 and Asp23 hydrogen bond (criteria listed in caption of Fig. S3) to relate side chain conformational sampling to hydrogen bond formation (black spikes in E and F), and ultimately dipole moment response. Panel (A) is replicated from main text Fig. 2F for ease of comparison.

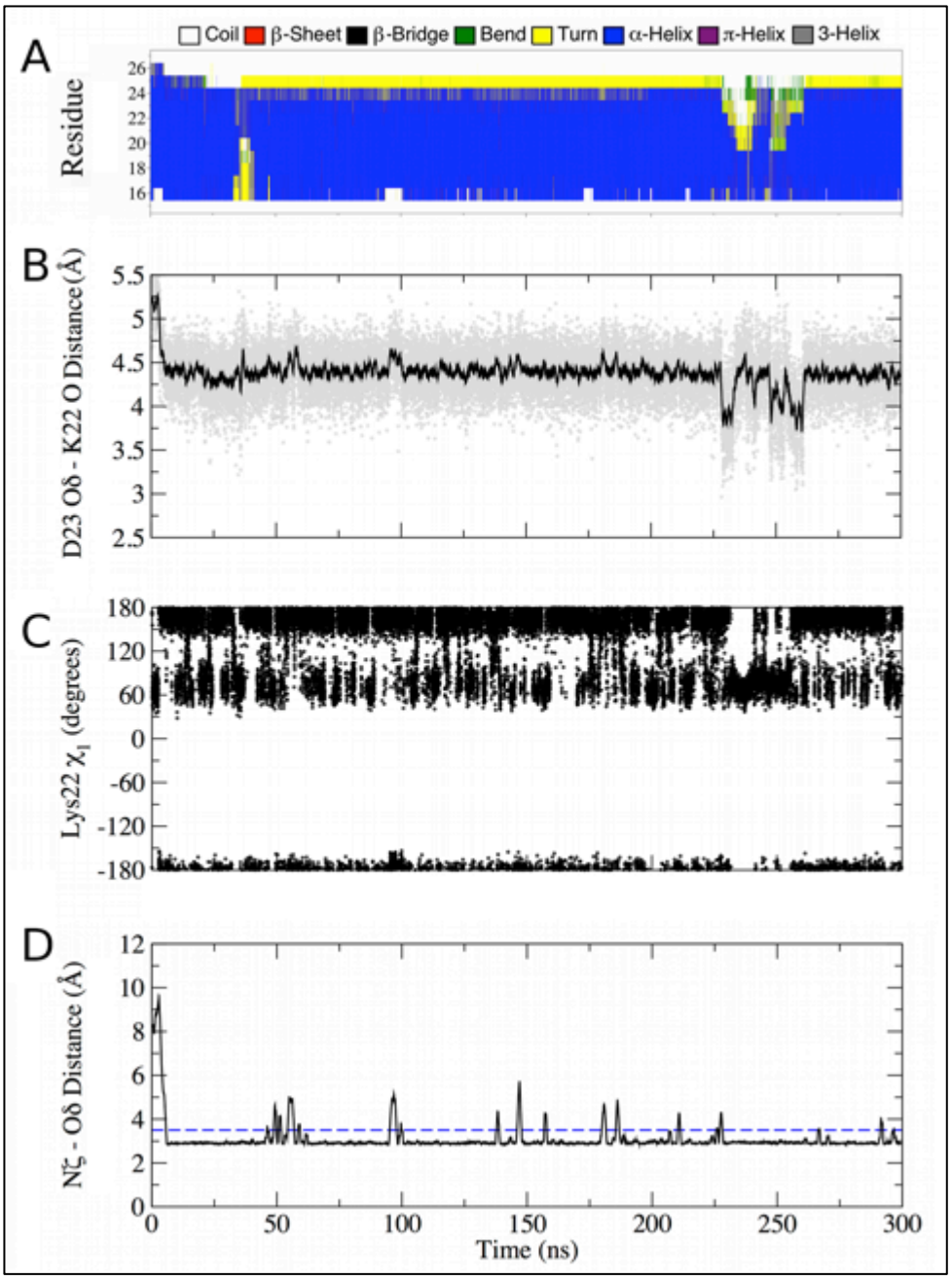


**Figure S6.** Dynamics of E22K $A\beta_{15-27}$ in ethanol. (A) Secondary structure evolution according to the DSSP algorithm. (B) Time series of the minimum distance between Asp23 Oδ atoms and Lys22 carbonyl O. Distances in each frame are shown as gray points, with a 1-ns running average shown as a black line. (C) Time series of Lys22 $\chi_1$. (D) Time series of minimum distance between the Lys22 Nζ and Asp23 $O\delta_1/O\delta_2$ atoms shown as a 1-ns running average for clarity. A value ≤ 3.5 Å (dashed blue line) for the Lys22 Nζ - Asp23 $O\delta_1/O\delta_2$ distance was used as an indicator of an intact salt bridge.

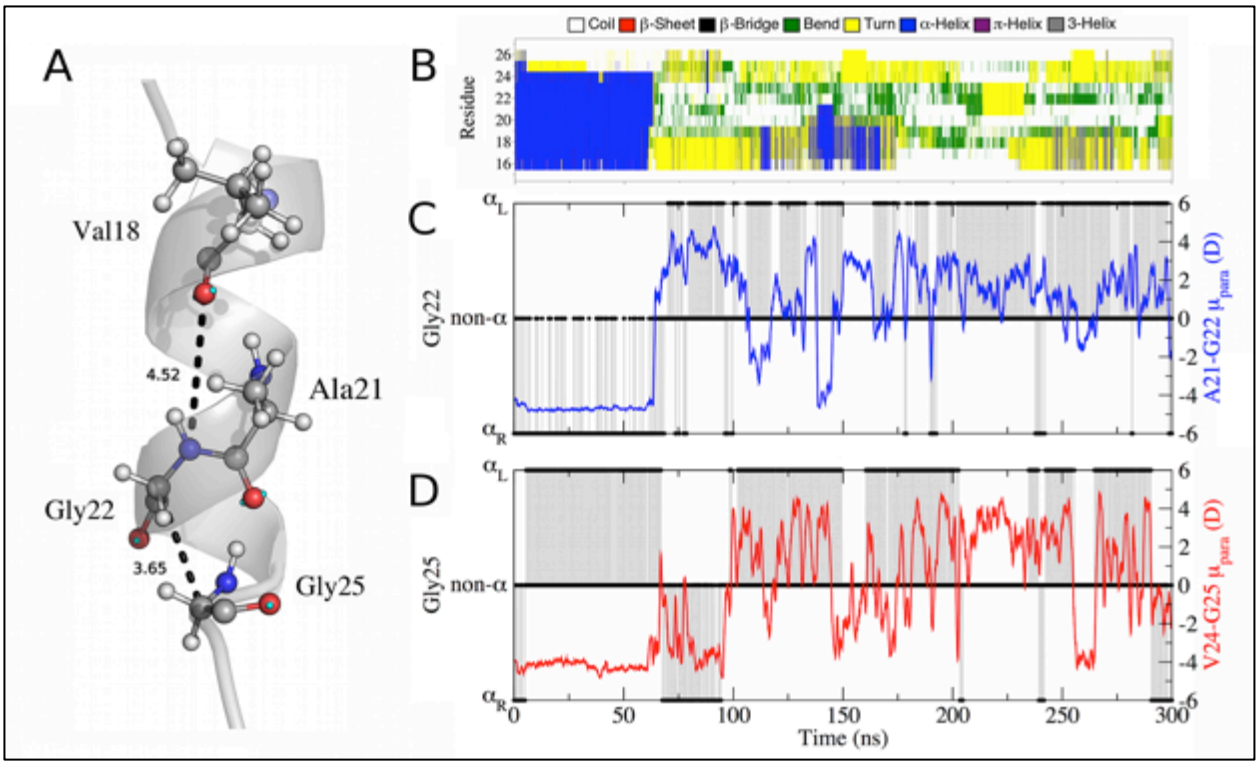


**Figure S7.** Unfolding of E22G $A\beta_{15-27}$ in water. (A) Helical distortion due to Gly22-Gly25 packing described in the main text. The Cα atoms of each Gly residue form close contacts (in this snapshot, 3.65 Å at 32.94 ns), leading to perturbed backbone hydrogen bonds, such as the between Val18-Gly22 (broken in this snapshot) and Ala21-Gly25 (perturbed here such that it deviates from linearity by 30°, broken at ~65 ns upon reversal of $\mu_{para}$). Deviation of Gly25 from alignment with the helix axis at 32.94 ns persists for ~30 ns forming a metastable, kinked helix. (B) Secondary structural evolution according to DSSP. Time series of $\mu_{para}$ for the (C) Ala21-Gly22 and (D) Val24-Gly25 peptide bonds, shown as 1-ns running averages and as a function of helical conformation; $\alpha_R$ was defined as ($-100° < \phi < -30°$, $-67° < \psi < -7°$) and $\alpha_L$ as ($30° < \phi < 100°$, $7° < \psi < 67°$), with "non-α" corresponding to any region on the Ramachandran surface that did not fall into these α definitions. The simultaneous $\alpha_R$-$\alpha_L$ conversion of Gly22 (C) and $\alpha_L$-$\alpha_R$ of Gly25 (D) leads to the reversal of $\mu_{para}$ at ~65 ns in (D) and complete loss of helicity shown in (B). In panels (C) and (D), the structural assignment in each frame is indicated by a black dot, connected by gray lines to illustrate the transitions between the different conformations.

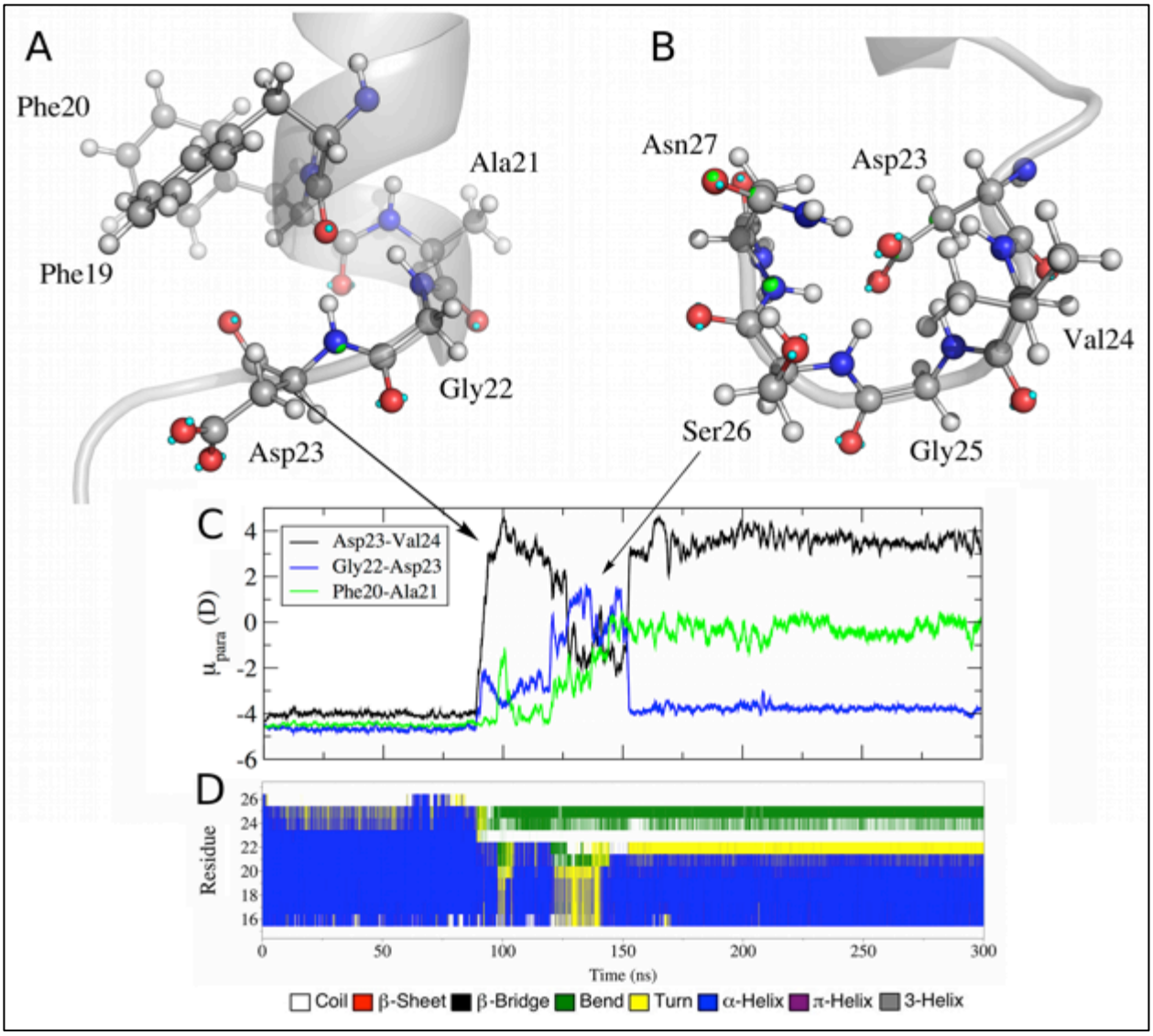


**Figure S8.** Partial unfolding of E22G A$\beta_{15\text{-}27}$ in ethanol. (A) Snapshot from 95.80 ns illustrating the rotation of Asp23 about its backbone $\phi$ dihedral to orient its carbonyl group in opposition to the helix axis. (B) Snapshot from 137 ns illustrating the stabilization of the anionic carboxylate of Asp23 by nearby amide groups due to the compaction of the backbone around Gly25. (C) Time series of $\mu_{para}$ of the indicated peptide bonds. (D) Secondary structure evolution according to DSSP. The reversal in direction of the Asp23-Val24 $\mu_{para}$ corresponds to the behavior illustrated in panel (A) and the disorder resulting from $\mu_{para}$ dynamics in the other peptide-bond dipole moments results in the transient loss of helicity shown in panel (D) when Asp23 is stabilized as shown in panel (B). Arrows to events in the $\mu_{para}$ time series in panel (C) correspond to the approximate frames in the time series illustrated in panels (A) and (B).

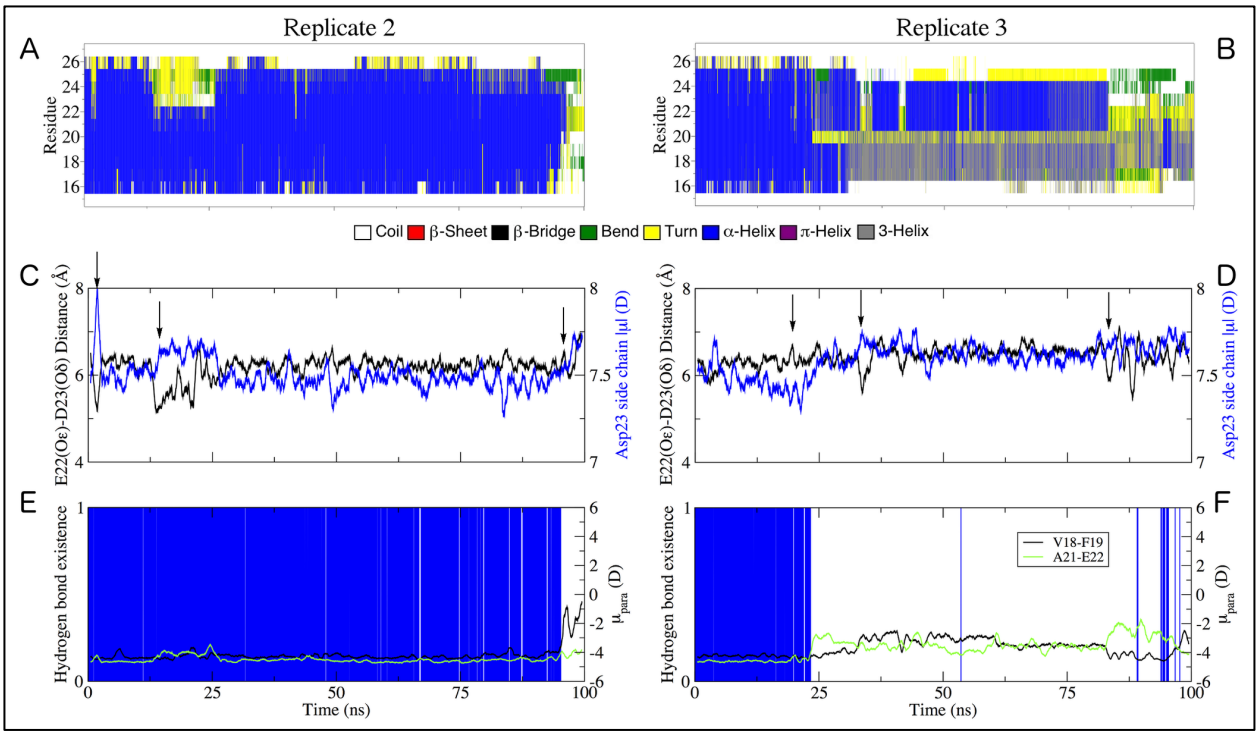


**Figure S9.** Unfolding of WT A$\beta_{15\text{-}27}$ in water. Shown are the results of the two additional 100-ns Drude simulations initiated with different velocities. (A,B) Secondary structure evolution according to DSSP. (C,D) Relationship between the Glu22-Asp23 side-chain minimum distance and Asp23 side chain dipole moment; arrows indicate close contacts with subsequent increases in side-chain |μ|. (E,F) Val18 to Glu22 *i* to *i*+4 backbone hydrogen bond existence (blue spikes indicate the presence of a hydrogen bond, i.e. existence = 1) and time series of $\mu_{para}$ for the indicated peptide bonds.

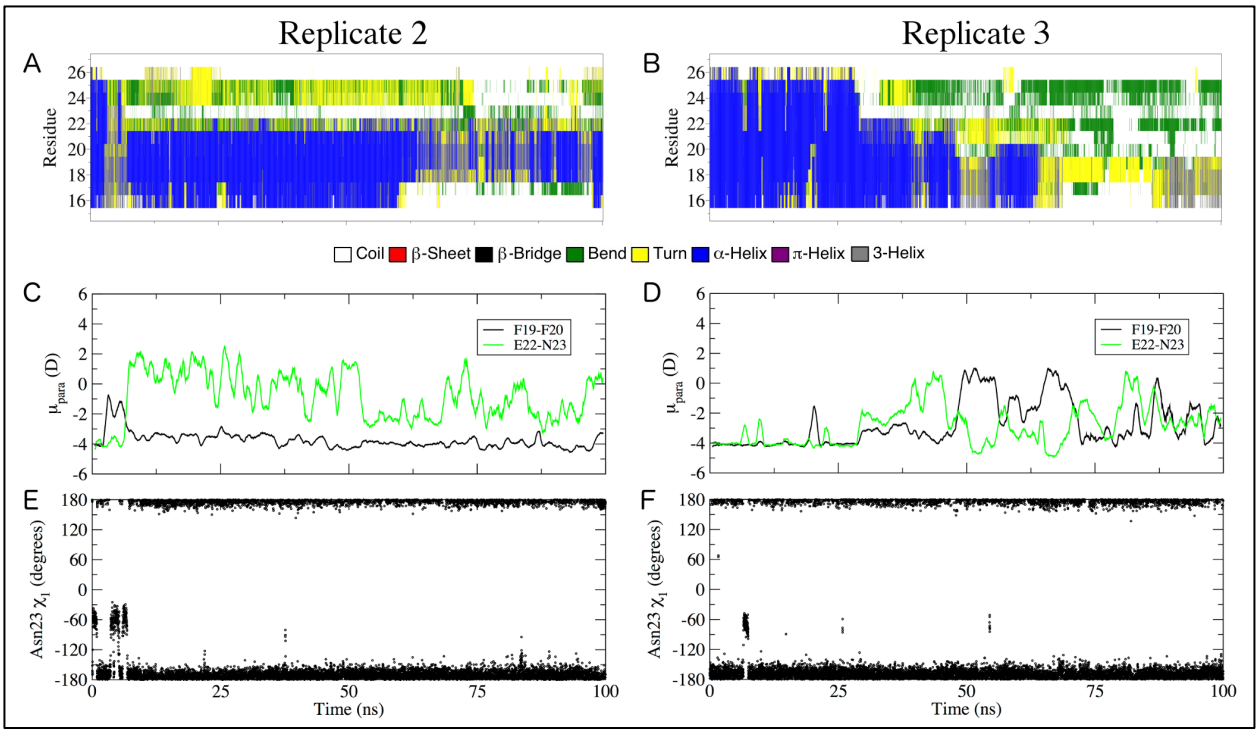


**Figure S10.** Unfolding of D23N A$\beta_{15-27}$ in water. Shown are the results of the two additional 100-ns simulations initiated with different velocities. (A,B) Secondary structure evolutions according to DSSP. (C,D) Time series of $\mu_{para}$ for the peptide bonds involved in hydrogen bond exchange. (E,F) Side chain $\chi_1$ time series for Asn23. Infrequent transitions of Asn23 $\chi_1$ to the $g^-$ rotamer coincide with transient destabilization of the helical turn encompassing Asn23 and ultimately the rest of the peptide.

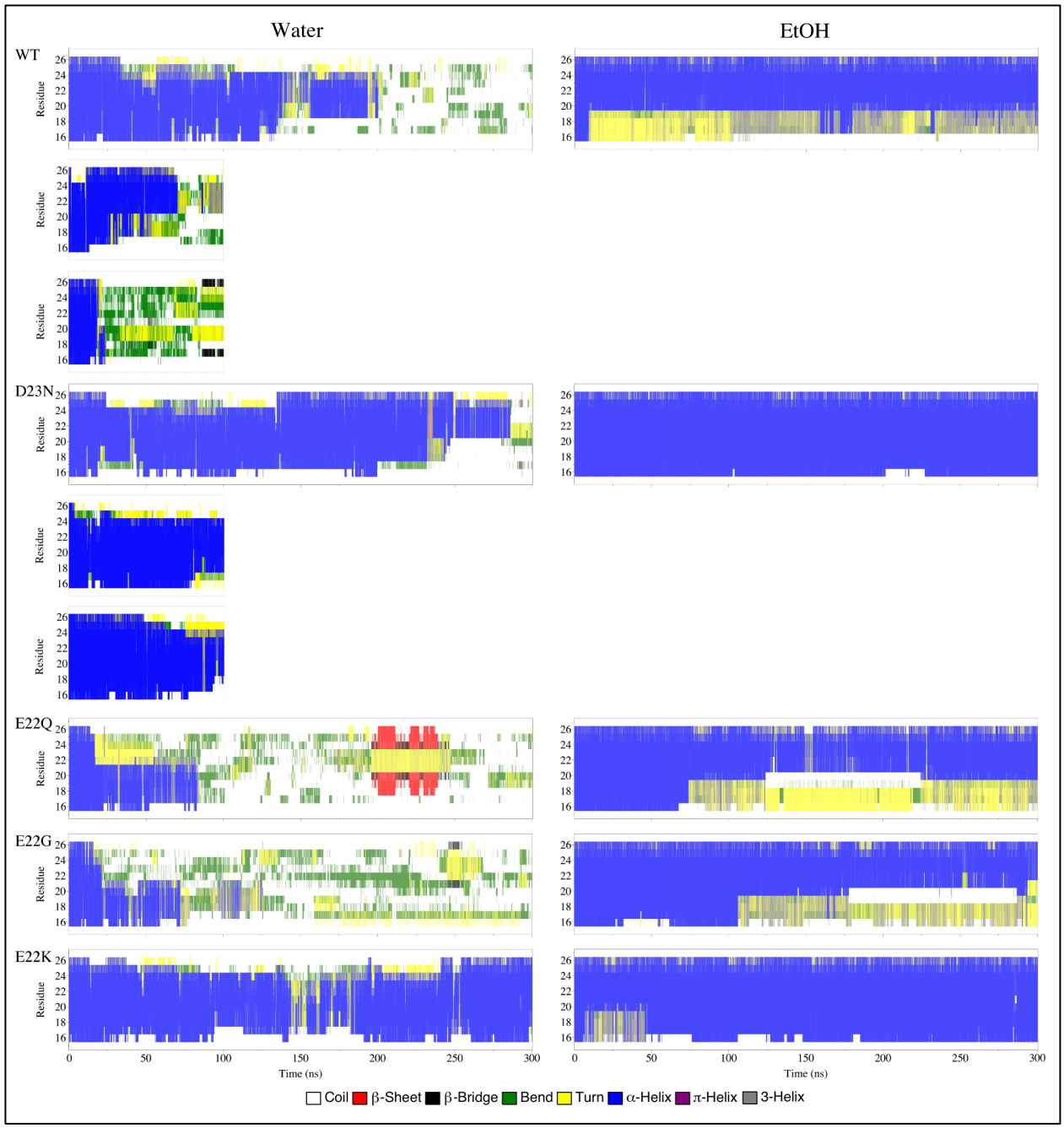


**Figure S11.** Secondary structure evolution according to DSSP for all $A\beta_{15-27}$ peptides using the additive CHARMM36 force field.

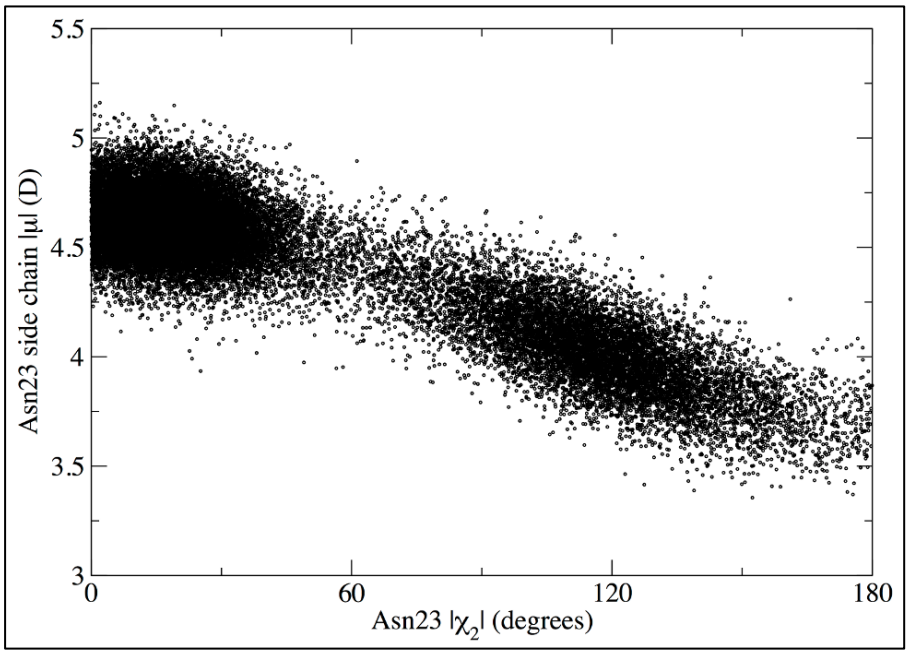


**Figure S12.** Side-chain dipole moment of Asn23 in the D23N $A\beta_{15-27}$ peptide in water from the additive CHARMM36 simulation as a function of the absolute value of the side-chain $\chi_2$ dihedral, from the 300-ns simulation. The calculated Pearson $\rho$ is -0.89 for the data sets, indicating that nearly all observed variation in the side-chain dipole moment is due to rotation about the $\chi_2$ dihedral and thus a reorientation of the amide group, rather than a response to the electric field.